

Random Mass Dirac Fermions in Doped Spin–Peierls and Spin–Ladder systems: One–Particle Properties and Boundary Effects

M. Steiner^(a), M. Fabrizio^(b), and Alexander O. Gogolin^(a)

^(a)*Imperial College, Department of Mathematics, 180 Queen’s Gate, London SW7 2BZ, U.K.*

^(b)*International School for Advanced Studies Via Beirut 4, 34014 Trieste, Italy
and Istituto Nazionale della Fisica della Materia INFN, Italy*

(March 22, 2021)

Abstract

Quasi–one–dimensional spin–Peierls and spin–ladder systems are characterized by a gap in the spin–excitation spectrum, which can be modeled at low energies by that of Dirac fermions with a mass. In the presence of disorder these systems can still be described by a Dirac fermion model, but with a random mass. Some peculiar properties, like the Dyson singularity in the density of states, are well known and attributed to creation of low–energy states due to the disorder. We take one step further and study single–particle correlations by means of Berezinskii’s diagram technique. We find that, at low energy ϵ , the single–particle Green function decays in real space like $G(x, \epsilon) \propto (1/x)^{3/2}$. It follows that at these energies the correlations in the disordered system are strong – even stronger than in the pure system without the gap. Additionally, we study the effects of boundaries on the local density of states. We find that the latter is logarithmically (in the energy) enhanced close to the boundary. This enhancement decays into the bulk as $1/\sqrt{x}$ and the density of states saturates to its bulk value on the scale $L_\epsilon \propto \ln^2(1/\epsilon)$. This scale is different from the Thouless localization length $\lambda_\epsilon \propto \ln(1/\epsilon)$. We also discuss some implications of these results for the spin systems and their relation to the investigations based on real–space renormalization group approach.

I. INTRODUCTION

One–dimensional quantum electron (and spin) systems have attracted considerable attention of theorists over the decades. The interest to these systems have been particularly boosted in recent years by the rapid development of experimental techniques. The latter include the discovery of various non–organic quasi–one–dimensional compounds. In particular, the materials we shall be concerned with in this paper are the recently discovered $GeCuO_3$ spin–Peierls compounds¹ and the spin–ladder compounds $(VO)_2P_2O_7$ and $SrCu_2O_3$ ². The modern experimental techniques allow measurements on these inorganic compounds, which were either impossible or inaccurate with the organic spin–Peierls materials in the past. These measurements not only can be now performed on single crystals, but also involve

controlled doping by impurities. The latter possibility brings up the old issue of the disorder effects in one-dimensional systems: a fascinating subject which was considered in the past as being somewhat academic.

Among various one-dimensional disordered systems, random exchange spin chains have been studied, using the so-called real-space renormalization group, with very intriguing results³⁻⁵. In particular, it has been shown⁴ that the typical behavior of the correlation functions may be quite different from the average behavior, which is more relevant from the experimental point of view. For instance, while the typical correlation functions usually decay exponentially, the average ones can be power law decaying. Moreover, even when the average correlation functions decay exponentially, the correlation length is different (bigger) from that of the typical correlations⁵. This feature is a consequence of rare disorder configurations dominating the long distance behavior of the correlation functions. The analogy of these spin systems with the effective disordered fermionic models have not been investigated in detail.

In this paper we shall partly fill this gap, and investigate more deeply the fermionic models. The main reason is that fermions naturally appear in the description of pure spin-Peierls chains and especially in the spin ladders. Moreover, this alternative approach is somewhat complementary to the real space renormalization group analysis, thus together they would provide a complete and satisfying description of such disordered systems.

Specifically, considering that both the spin-Peierls and the spin-ladder systems have a spin gap in the excitation spectrum, it is not surprising that the effective fermionic model for both systems is a model of massive Dirac fermions. The effect of non-magnetic impurities is to randomize the mass (see also the next Section). Thus, the ultimate fermionic model, on which we focus in what follows, is the one-dimensional random mass Dirac fermion model.

A great deal is known about simple self-averaging quantities for this model, like the total density of states and the localization length.

For a Gaussian (white noise) distribution of the mass variable $m(x)$ the density of states was calculated by Ovchinnikov and Erikhman⁶. Using Fokker-Planck type equations for the probability distribution of the wave-function phase, they obtained the divergent density of states⁷,

$$\rho(\epsilon) \propto \frac{1}{|\epsilon \ln^3(1/\epsilon)|}, \quad (1)$$

as the energy approaches the midgap $\epsilon \rightarrow 0$.

Physically, the appearance of the singularity in the density of states can be easily understood. Indeed, for a single kink (sign change) of the mass, there always is a zero-energy bound state, localized around the point in space where $m(x) = 0$. For many kinks, there are many such localized states (also referred to in the literature as zero-modes or solitons). If they were not overlapping, the density of states would have a δ -function peak at $\epsilon = 0$. In fact the zero-modes are overlapping. Hence the δ -peak broadens, but the singularity remains - Eq.(1). [In order to give a qualitative explanation as to why the broadened δ -peak takes exactly the shape (1), a more elaborated argumentation is needed: see, e.g., Ref. 7.] It must be noted that the singularity in the density of states of the form (1) has been discovered by Dyson back in 1953⁸ for a model of a disordered harmonic chain. In the electronic spectrum at the center of the Brillouin zone such a singularity was identified by Weissman

and Cohan⁹ for the case of an off-diagonal disorder (random hopping model). The latter model is in fact directly related to the random mass Dirac problem.

According to the Thouless relation¹⁰, the localization length corresponding to the density of states (1) takes the form

$$\lambda_\epsilon \sim l \ln(1/\epsilon) , \quad (2)$$

where l is the mean free path. The fact that the localization length diverges in the middle of the gap makes the random mass Dirac problem different from the usual one-dimensional localization problem. For the latter, the localization length essentially coincides with the mean free path l , so that there is only one length scale in the problem. Consequently, it makes sense to consider only the distances $x \gg l$ where the correlation functions decay exponentially¹¹. On the contrary, for the random mass Dirac fermions, various length scales come into play: the mean free path l , the localization length λ_ϵ , and what we shall call the correlation length L_ϵ . We are going to argue that

$$L_\epsilon \sim l \ln^2(1/\epsilon) .$$

(This is in agreement with the renormalization group studies, mentioned above; see also Section VI.) The correlation length diverges even faster than the localization length. While we do expect that the correlation functions for the random mass Dirac fermion model behave in the same way as those for standard one-dimensional disordered systems at distances $x \gg L_\epsilon$, there is a different regime $l \ll x \ll L_\epsilon$, arising at low energies. A new physics emerges in this regime, the understanding of which this paper is intended to contribute to. Specifically, the system seems to exhibit some kind of criticality – all the known correlation functions are power-law decaying with universal exponents. This behavior is determined by rare fluctuations when the particle wave-functions have large amplitudes.

As we already mentioned, the simple self-averaging quantities, like the total density of states, can be computed by various methods like the Fokker-Planck type equations for the probability distributions or the replica trick¹². All these methods are, however, ill-suited for determining the correlation functions. In their recent preprint Shelton and Tsvelik succeeded to make use of an elegant mapping of the Dirac problem at zero energy ($\epsilon = 0$) onto the so-called Liouville quantum mechanics¹³ for calculating the disorder averages of the products $\psi_0^2(x_1)\psi_0^2(x_2)\dots\psi_0^2(x_N)$ of the zero-energy wave-function amplitudes. While this mapping does provide an interesting insight into the random mass Dirac problem (strictly) at zero energy, we are interested to get more information about the correlation functions, in particular about the correlations involving the phase of the wave-functions and about their energy dependence.

On the other hand, a method, which does (in principle) allow to calculate all the correlation functions, has been around for almost 25 years. The method is the Berezinskii diagram technique originally invented (back in 1973) to confirm the Mott hypothesis of $\omega^2 \ln \omega$ vanishing conductivity for the standard one-dimensional localization problem¹¹. The Berezinskii method was extended by A.A. Gogolin and Mel'nikov (GM)¹⁴ to the case of a half-filled electron band with a random backscattering, the model equivalent to the random mass Dirac fermions. Needless to say that GM were able to reproduce the Dyson singularity in the density of states. More importantly, they calculated the current-current and the

density–density correlation functions. The current–current correlation function has no apparent physical meaning for the spin systems. From the point of view of the latter, the density–density correlation function is more interesting, for it turns out to be proportional to the staggered susceptibility (at least for spin–Peierls systems, see also below). GM found that, in the region $l \ll x$, the contribution to the density–density correlation function at low frequency ω of the state with energy ϵ such that $x \ll L_\epsilon$ decays as

$$\langle \psi_{\epsilon+\omega}^\dagger(x) \psi_\epsilon(x) \psi_\epsilon^\dagger(0) \psi_{\epsilon+\omega}(0) \rangle \propto \left(\frac{1}{x}\right)^{3/2}. \quad (3)$$

(This asymptotics was reproduced by Shelton and Tsvelik¹³ for $\epsilon = \omega = 0$).

In this paper we further study the random mass Dirac problem following the line pioneered by GM. After defining the model and discussing its relation to spin systems, we briefly introduce the Berezinskii technique (we feel that that would be convenient for the reader since a transparent explanation of the Berezinskii technique is often neglected in the literature). Then we apply the technique to the calculation of the single–particle Green function at low energy. Amusingly, we find that the Green function decays as $(1/x)^{3/2}$ (for $l \ll x \ll L_\epsilon$). Namely, it is characterized by the same exponent as the density–density correlation function.

In the second part of the paper we study a somewhat different (though related) question. Namely, we calculate the local density of states in the presence of a boundary. Unlike the case of the usual localization [for which the effects of boundaries were studied by Al’tshuler and Prigodin (AP)¹⁵], for the random mass Dirac problem one might expect that the boundaries affect already the average local density of states (and not just its distribution function). Indeed, it turns out that the Dyson singularity is enhanced close to the boundary as $\ln(1/\epsilon)$, as compared to its bulk value. The local density of states then decays into the bulk of the sample following the law $1/\sqrt{x}$, and finally saturates to the bulk value at $x \sim L_\epsilon$. We also confirm these results by a real–space renormalization group analysis. Some consequences for the thermodynamics of the spin systems are discussed in the last Section.

We would like to stress that, despite all the results mentioned above, we are just starting to study the problem in this paper. Ultimately, a comprehensive understanding of the new physics, arising in the random mass Dirac problem will only be achieved when the fluctuations of the correlation functions are understood. The problem is mathematically involved, so that, unlike the usual case¹⁵, even the distribution function of the simplest quantity, the local density of states, is unknown at present. We hope to return to these questions in future publications¹⁶.

II. THE MODEL

The one–dimensional Dirac Hamiltonian is of the form

$$H_D = \int dx \{ v \Psi^\dagger (-i \partial_x) \sigma_z \Psi + m(x) \Psi^\dagger \sigma_x \Psi \}, \quad (4)$$

where σ_x, σ_z are the Pauli matrices, and $\Psi^\dagger(x) = [R^\dagger(x), L^\dagger(x)]$. The operators $R(x)$ [$L(x)$] stand for the chiral right (left) moving electron fields. The mass term $m(x)$ is randomly

distributed. Throughout this paper we shall assume $m(x)$ be Gaussian with vanishing average: $\langle m(x) \rangle = 0$. Its distribution is therefore determined by the correlation function

$$\langle m(x)m(x') \rangle = \frac{v^2}{l} \delta(x - x') , \quad (5)$$

where l is the mean free path (and v is the velocity).

In practice, the Dirac model (4) usually arises as a continuum version of a lattice model, so that R and L are the chiral components of the continuum limit for a lattice electron field operator

$$\psi_n \rightarrow e^{ik_F x} R(x) + e^{-ik_F x} L(x), \quad \text{for } x = na_0 . \quad (6)$$

Here a_0 is the lattice spacing and the condition of being at the half-filling for the lattice model means that $4k_F a_0 = 2\pi$. From (6) it is clear that (4) is just another way to write down the random backscattering electron model at half-filling.

Notice that there is no forward scattering in the problem. This is rigorously true for a simple tight-binding model at half-filling with random nearest-neighbor hopping integrals. This model is particle-hole symmetric

$$\psi_n \rightarrow (-1)^n \psi_n^\dagger,$$

which prevents any generation of forward scattering processes. Hence this model in the continuum limit would reproduce the Hamiltonian (4).

The Hamiltonian (4) has been shown to also describe the low-energy limit of one-dimensional spin systems with a spin gap in the excitation spectrum (see Refs 17,18). For the convenience of the reader we shall present the qualitative side of the argument.

- Spin-Peierls systems. The spin part of the Hamiltonian for a single spin-1/2 chain interacting with phonons takes the form

$$H_{\text{SP}} = \sum_n J \vec{S}_n \vec{S}_{n+1} + \sum_n \Delta_n (-1)^n \vec{S}_n \vec{S}_{n+1} , \quad (7)$$

where \vec{S}_n are spin-1/2 operators, J is the exchange coupling constant, and Δ_n measures the strength of the dimerization caused by the interaction with the phonons. Below the spin-Peierls transition temperature, one usually assumes $\Delta_n \rightarrow \langle \Delta_n \rangle = \Delta$ (the mean-field approach is appropriate for the phonons normally have a three-dimensional dispersion relation). The passage to the model (4) is as follows. The XY-version of the model (7) can be mapped onto a fermionic model in a standard way by using the Jordan-Wigner transformation. Taking the continuum limit leads to (4) with the parameter Δ determining the mass m_0 . The J_z coupling corresponds to a four-fermion interaction term, but it is irrelevant because of the spin gap. The main effect of the doping is to randomize the mass term $m(x)$. As argued in Ref. 17, a single impurity effectively introduces a domain wall into the system – a kink separating phases with different signs of the dimerization order parameter. The mass variable, proportional to the dimerization strength, will thus also have a kink at the domain wall position x_0 , changing from $m(x) = m_0$ for $x < x_0$ to $m(x) = -m_0$ for $x > x_0$.

- Spin-ladder systems. The Hamiltonian of two coupled spin-1/2 chains is

$$H_{\text{SL}} = \sum_{n,j=1,2} J \vec{S}_{n,j} \vec{S}_{n+1,j} + \sum_n J_{\perp} \vec{S}_{n,1} \vec{S}_{n,2}, \quad (8)$$

where the coupling between the chains, J_{\perp} , is assumed to be small (this is not qualitatively restrictive but allows one to construct a consistent theory). In the continuum limit description, the spin density operators on each chain have slow-varying components as well as fast (staggered) components:

$$\vec{S}_{n,j} \rightarrow \vec{S}(x) + (-1)^n \vec{n}_j(x). \quad (9)$$

The staggered correlations are stronger than the uniform correlations, so the most relevant interaction between the chains is

$$J_{\perp} a_0^{-1} \int dx \vec{n}_1(x) \cdot \vec{n}_2(x) \quad (10)$$

(other couplings are, in fact, marginal). The scaling dimension of the coupling (10) is equal to unity. Therefore, as it was realized by Shelton, Nersisyan, and Tsvelik¹⁹, this coupling can be conveniently re-fermionized. The result is the Dirac model (4) with the mass parameter proportional to coupling J_{\perp} ²⁰. Let us now discuss what the effect of doping would be. Consider, for example, the situation in $La_1CuO_{2.5}$ spin-ladder system doped by Sr (which substitutes La)²¹. For low Sr concentrations ($x < 0.02$), the holes (carrying spin-1/2's) are localized on the Oxygen atoms, i.e. in between neighboring sites of the Cu magnetic lattice. As a result the magnetic sites from the right of such an impurity are effectively re-numbered (shifted by one). Consequently, the staggered magnetization changes sign causing a sign change of the coupling (10) and of the mass term of the corresponding Dirac problem²².

Thus, the above considerations of the doping effects lead, for both the spin-Peierls and the spin-ladder systems, to the random mass Dirac model. Specifically, the mass turns out to be distributed as a random ‘telegraph signal’

$$m(x) = m_0 \prod_i \text{sgn}(x - x_i), \quad (11)$$

x_i being randomly distributed. At low energies (namely at energies well below the gap: $\epsilon \ll m_0$), the model is still equivalent to the one with a Gaussian distribution of the mass⁷. Since we are mainly interested in the asymptotic behavior of the correlation functions (i.e., in the parameter region where the correlation functions are expected to be universal: $\epsilon \ll m_0$ while $l \ll x \ll L_{\epsilon}$), we can safely assume the Gaussian distribution. Then the correlation functions can be calculated by means of the Berezinskii diagram technique¹¹ introduced in the following Section.

III. BEREZINSKII DIAGRAM TECHNIQUE

The Berezinskii technique is based on the perturbation theory for the one-particle Schrödinger equation (rather than on the many-body perturbation theory). Consider a translationally invariant one-particle Hamiltonian \hat{H}_0 perturbed by a random potential (random mass) term \hat{m} . The bare retarded Green function in the energy representation is given by

$$\hat{G}^{0+} = \frac{1}{\epsilon - \hat{H}_0 + i\delta} . \quad (12)$$

The exact Green function for a given realization of the disorder is defined as

$$\hat{G}^+ = \frac{1}{\epsilon - \hat{H}_0 - \hat{m} + i\delta} . \quad (13)$$

This Green function satisfies the equation

$$\hat{G}^+ = \hat{G}^{0+} + \hat{G}^{0+} \hat{m} \hat{G}^+ . \quad (14)$$

Iterating (14) one obtains a standard perturbative expansion for the Green function. A typical term of the perturbative series is of the form

$$\hat{G}^{0+} \hat{m} \hat{G}^{0+} \hat{m} \hat{G}^{0+} \dots \hat{G}^{0+} \hat{m} \hat{G}^{0+} . \quad (15)$$

The next step is to take the disorder average. Clearly only the $2n$ -th order terms survive (i.e., the terms containing an even number of impurity potentials). The disorder average $\langle m(x_1)m(x_2)\dots m(x_{2n}) \rangle$ is then given by a sum of products of all possible pair correlators (5). (An additional matrix structure of the mass term simply ensures that the left- and right movers are interchanged in every scattering event.) For example, at second order there is just one term

$$\int dx_1 G^{0+}(x', x_1) G^{0+}(x_1, x_1) G^{0+}(x_1, x) \quad (16)$$

(The usage of the coordinate rather than the momentum representation is vital, as it will become clear shortly.) At fourth order there are two terms and two integration variables, etc..

Let us now represent these contributions to the Green function graphically. The bare electron Green functions are represented by solid lines. The disorder potential correlators by ‘interaction’ (wavy) lines, which shall always be vertically aligned. The term (16) for $x' < x_1 < x$ is then given by the graph Fig.1(a). This graph is also an example of an elementary ‘interaction’ vertex. Other contributions are represented by more complicated diagrams where several vertices Fig.1(a) and (or) other vertices are joined. An elementary consideration of the scattering processes described by the model (4) shows that Fig.1(a-d) exhausts all the possible vertices. Using the many-body terminology, there are no forward scattering vertices [simply because there is no scattering within the same chiral branch in (4)]. The vertices Fig.1(c,d) are referred to in the literature as umklapp scattering vertices.

It is very important that, by construction, the diagrams are x -ordered: $x_1 < \dots x_i < x' < x_{i+1} < \dots < x_j < x < x_{j+1} < \dots < x_{2n}$ ²³.

As we have already stressed, each scattering event interchanges the right- and the left-moving electrons. The bare Green functions for them are given by

$$G_R^{0+}(x', x; \epsilon) = -\frac{i}{v}\theta(x' - x)e^{i\frac{\epsilon}{v}(x-x')}, \quad G_L^{0+}(x', x; \epsilon) = -\frac{i}{v}\theta(x' - x)e^{i\frac{\epsilon}{v}(x'-x)}, \quad (17)$$

where $\theta(x)$ is the step function. Alternatively, one can use the bare Green function of the combined electron field (6)

$$G^{0+}(x', x; \epsilon) = e^{ik_F(x-x')}G_R^{0+}(x', x; \epsilon) + e^{-ik_F(x-x')}G_L^{0+}(x', x; \epsilon) = -\frac{i}{v}e^{i(k_F+\frac{\epsilon}{v})|x-x'|}. \quad (18)$$

The next important observation is that, since all the diagrams are space-ordered, the Green functions (17,18) are actually factorized in each given graph. This enables one to split the unperturbed Green function $G^{0+}(x_i, x_j; \epsilon) = -\frac{i}{v}\exp\left[i(k_F + \frac{\epsilon}{v})(x_j - x_i)\right]$ (for $x_j > x_i$) into two factors $\exp\left[-i(k_F + \frac{\epsilon}{v})x_i\right]$ and $\exp\left[+i(k_F + \frac{\epsilon}{v})x_j\right]$, and to assign the coordinate dependence only to the vertices and to the end points, not to the lines. As a result, the solid lines just tell us how the vertices are joined: the analytic expression for any graph is given by a product of the vertex (and end point) factors. Note that the factors corresponding to the vertices Fig.1 (a,b), $-1/(2l)^{24}$ and $-1/l$ respectively, are x -independent. The factors $(-1/l)\exp[\pm i(\epsilon/v)x]$ corresponding to the vertices Fig.1 (c,d) also weakly depend on x (as $\epsilon \rightarrow 0$). The reason is that the Fermi wave-vector k_F corresponds to half-filling: $e^{i4k_F x} = 1$. As it was realized by GM¹⁴, these (umklapp) vertices make the problem different from the standard localization problem. (At large energies, i.e. well away from half-filling, these vertices strongly oscillate and give a negligible contribution after integration over the spatial coordinates is performed¹¹.)

So far we have merely reformulated the problem. However, the cardinal idea of the Berezinskii methods is to provide a way of summing all the diagrams. The procedure is based on an ingenious classification of diagrams¹¹. Since each diagram is characterized by a fixed number of vertices in a definite spatial order, one can split it into a product of three integrals over the vertex contributions: the contributions from the region to the left of x' , those made in the region to the right of x , and those made in the central region (between x' and x). These integrals, which are referred to in the literature as ‘Berezinskii blocks’, are then classified by the number of lines passing through their boundaries. For instance, $\tilde{R}_m(x')$ is the sum of all contributions to the left of x' with $4m$ lines, and, equivalently, $R_m(x)$ defines the sum of all contributions to the right of x . By joining interaction vertices to Berezinskii’s block of a given order, one finds Berezinskii’s blocks of higher (and lower) order. This allows for recurrence relations to be derived. Instead of trying to give here a general description of the procedure, we shall illustrate the method at work while calculating the single-particle Green function in the next Section.

IV. SINGLE-PARTICLE GREEN FUNCTION

By multiplying the iteration series (15) with different energies (and spatial coordinates) and applying the Berezinskii method one can, in principle, calculate all the correlation

functions. So, the density–density (and current–current) correlation functions, which are two–particle correlation functions, were found by GM¹⁴ (see Section VI for discussion). In this paper we concentrate on the single–particle properties of the random mass Dirac problem. We thus apply the Berezinskii technique for calculating the single particle Green function $G^+(x', x; \epsilon)$.

A. Basic equations

We start classifying the graphs contributing to the single–particle Green function by considering all possible end point configurations. Since the electron line can be drawn either to the left or to the right of each of the two end points x', x , there are four possible configurations, as shown in Fig.2. In going along a diagram, the number of the electron lines passing through the current vertical cross section of the digram may be changed (by some amount Δg) when one encounters an interaction vertex. So, the vertices Fig.1(a,b) do not change the number of lines, $\Delta g = 0$. The vertices Fig.1(c,d) do change the number of lines by $\Delta g = \pm 4$. An elementary analysis shows that the end point configurations Fig.2(c,d) would require $\Delta g = \pm 2$. This is impossible with the set of elementary vertices at our disposal. So, the configurations Fig.2(c,d) do not contribute to the Green function.

We are therefore left with the two end point configurations Fig.2(a,b). The structure of the Berezinskii blocks corresponding to these configurations is shown in Fig.3(a,b). The \tilde{R} and R blocks can only have multiple of 4 number of the electron lines. They are therefore identical for both configurations Fig.3(a,b). On the other hand, the central blocks $Z^{(a)}$ and $Z^{(b)}$ differ. Indeed, given the left–hand–side block $\tilde{R}_{m'}$ has $4m'$ lines and the right–hand–side block R_m has $4m$ lines, the central block Z^a must have $4m' + 1$ ($4m + 1$) lines on the left (right) while the central block Z^b must have $4m' - 1$ ($4m - 1$) lines on the left (right). [Thus, $m \geq 0$ for a –configuration while $m \geq 1$ for b –configuration.]

In terms of the Berezinskii blocks the single–particle Green function is expressed as follows ($x' < x$)

$$G^+(x', x) = -\frac{i}{v} \left\{ \sum_{m,m'=0}^{\infty} \tilde{R}_{m'}(x') Z_{m',m}^{(a)}(x', x) R_m(x) + \sum_{m,m'=1}^{\infty} \tilde{R}_{m'}(x') Z_{m',m}^{(b)}(x', x) R_m(x) \right\}. \quad (19)$$

Consider now the Green function for coinciding points $x' = x = 0$. When the end points merge, the region of the spatial integration in the central blocks collapses so that only the trivial diagrams for $Z^{(a,b)}$ survive (those which do not include any interaction vertices). Hence the boundary conditions

$$Z_{m',m}^{(a,b)}(x = 0, x) = \delta_{m',m} \text{ for } m \geq 0(1). \quad (20)$$

For an infinite sample, the boundary conditions to be imposed on R_m 's are

$$\tilde{R}_0(x) = R_0(x) = 1. \quad (21)$$

Thus, the equal–point Green function is given by

$$G^+(x-0, x) = -\frac{i}{v} \left\{ 1 + 2 \sum_{m=1}^{\infty} \tilde{R}_m(x) R_m(x) \right\}. \quad (22)$$

The local density of states is defined as

$$\rho(x, \epsilon) = -\frac{1}{\pi} \text{Im} G^+(x-0, x; \epsilon). \quad (23)$$

In an infinite system the quantities (22) and (23) do not actually depend on x , for the disorder average effectively restores translation invariance. (The situation is different for systems with boundaries we discuss in Section V.) Note the appearance of the factor of two in front of the sum in the equation (22). This factor is due to configurations Fig.2 mirror imaging each other when the end points merge, as illustrated in Fig.5.

The expression (23) was used by GM for calculating the density of states. They found the following differential recurrence relation for the Berezinskii blocks \tilde{R}_m

$$\begin{aligned} \frac{d\tilde{R}_m(x)}{dx} = & -\frac{1}{l} \left\{ 4m^2 \tilde{R}_m(x) + m(2m-1) e^{-i\frac{4\epsilon}{v}x} \tilde{R}_{m-1}(x) \right. \\ & \left. + m(2m+1) e^{-i\frac{4\epsilon}{v}x} \tilde{R}_{m+1}(x) \right\}. \end{aligned} \quad (24)$$

The right-hand-side blocks $R_m(x)$ mirror the blocks $\tilde{R}_m(x)$, so they satisfy (24) with $x \rightarrow -x$. An integral equation equivalent to the equation (24) is obtained by joining the elementary vertices to $\tilde{R}_m(x)$ in all possible ways, but avoiding creation of closed electron loops. (The loop diagrams are not allowed because we study a one-particle problem. Put another way, they vanish because they involve a retarded Green function.) The process is illustrated in Fig.4. The first term in (24) comes from joining the vertices Fig.1(a,b)

$$4m^2 = \frac{1}{2} 4m + 2m(2m-1).$$

The second and the third term derive from joining the vertices Fig.1(c) and (d) respectively.

Carrying out an analogous calculation (Fig.4) for the central blocks $Z^{(a,b)}$, we obtained the differential recurrence relations satisfied by these blocks (in computing the integer coefficients one must be careful as to not allowing for the electron loops in the whole diagram):

$$\begin{aligned} \frac{dZ_{*,m}^{(a)}(x)}{dx} = & i\frac{\epsilon}{v} Z_{*,m}^{(a)}(x) - \frac{8m^2 + 4m + 1}{2l} Z_{*,m}^{(a)}(x) \\ & - \frac{m(2m-1)}{l} e^{-i\frac{4\epsilon}{v}x} Z_{*,m-1}^{(a)}(x) - \frac{(m+1)(2m+1)}{l} e^{i\frac{4\epsilon}{v}x} Z_{*,m+1}^{(a)}(x) \end{aligned} \quad (25)$$

and

$$\begin{aligned} \frac{dZ_{*,m}^{(b)}(x)}{dx} = & -i\frac{\epsilon}{v} Z_{*,m}^{(b)}(x) - \frac{8m^2 - 4m + 1}{2l} Z_{*,m}^{(b)}(x) \\ & - \frac{(m-1)(2m-1)}{l} e^{-i\frac{4\epsilon}{v}x} Z_{*,m-1}^{(b)}(x) - \frac{m(2m+1)}{l} e^{i\frac{4\epsilon}{v}x} Z_{*,m+1}^{(b)}(x) \end{aligned} \quad (26)$$

Only the active spatial variable x is shown (the variable x' is suppressed), $*$ stands for the index m' which plays a role of a parameter. Defining the Berezinskii blocks [c.f. (19)], we

have incorporated the end point exponentials $\exp\left(\pm i\frac{\epsilon}{v}x\right)$ into $Z^{(a,b)}$. Hence the first terms on the right-hand-side of the above equations. [The absence of $e^{\pm ik_F x}$ factors means that we are actually calculating G_R , the total Green function can be restored by using the formula (18).]

As a next step it is instructive to pass to the momentum representation for the Green function. Before doing so we notice that the spatial dependence of the side blocks can easily be separated¹⁴. Indeed, the substitution

$$\tilde{R}_m(x) = (-1)^m e^{-i\frac{4\epsilon}{v}mx} R_m \quad (27)$$

reduces the equations (24) and (21) to the algebraic recurrence relation

$$isR_m = 4mR_m - (2m-1)R_{m-1} - (2m+1)R_{m+1} \quad (28)$$

for the x -independent quantities R_m obeying the boundary condition

$$R_0 = 1. \quad (29)$$

We have introduced the dimensionless energy variable

$$s = \frac{4\epsilon l}{v}. \quad (30)$$

It will also be of convenience to pass to the dimensionless spatial coordinate

$$y = \frac{x}{l}. \quad (31)$$

Now we define the objects

$$Q_m^{(a,b)}(\kappa, s) = l(-1)^m \sum_{m'=0(1)}^{\infty} (-1)^{m'} \int_{y'}^{\infty} dy e^{-i\kappa(y-y') + is(my-m'y')} Z_{m',m}^{(a,b)}(ly', ly) R_{m'}. \quad (32)$$

The sum over m' in the above formula starts with 0 for a -configurations and with 1 for b -configurations respectively.

In terms of the objects (32), the Fourier transformed Green function takes the simple form

$$G_R(\kappa, s) = l \int_{y'}^{\infty} dy e^{-i\kappa(y-y')} G_R(ly', ly; s) = -\frac{i}{v} \left[\sum_{m=0}^{\infty} R_m Q_m^{(a)}(\kappa, s) + \sum_{m=1}^{\infty} R_m Q_m^{(b)}(\kappa, s) \right]. \quad (33)$$

Finally, applying the operation (32) to Eqs.(25,26) and using the boundary conditions (20), one can derive algebraic recurrence relations for $Q_m^{(a,b)}(\kappa, s)$. We found

$$is \left(m + \frac{1}{4} \right) Q_m^{(a)} - i\kappa Q_m^{(a)} - \frac{8m^2 + 4m + 1}{2} Q_m^{(a)} + m(2m-1)Q_{m-1}^{(a)} + (m+1)(2m+1)Q_{m+1}^{(a)} = R_m \quad (34)$$

and

$$\begin{aligned}
& is \left(m - \frac{1}{4} \right) Q_m^{(b)} - i\kappa Q_m^{(b)} - \frac{8m^2 - 4m + 1}{2} Q_m^{(b)} + \\
& (m-1)(2m-1)Q_{m-1}^{(b)} + m(2m+1)Q_{m+1}^{(b)} = R_m,
\end{aligned} \tag{35}$$

where we have suppressed the inactive variables (κ, s) .

B. Asymptotic solution of the equations

In order to compute the Green function we need to solve the recurrence relations (28,34,35) for the quantities R_m and $Q_m^{(a,b)}$ and use the formula (33).

As we already mentioned, the recurrence relation (28) for R_m 's was derived by GM. They also discovered that the generating function $R(\zeta) = \sum_m R_m \zeta^m$ satisfies a second order differential equation that happens to be of a hypergeometric type. It can therefore be explicitly solved by, e.g., contour integrals method. The solution found by GM reads¹⁴

$$R_m = \frac{e^{is/4}}{K_0(-is/4)} \int_0^\infty \frac{dt}{[t(t+1)]^{1/2}} \left(\frac{t}{t+1} \right)^m e^{ist/2}, \tag{36}$$

where K_0 is the MacDonal function. (It can be checked that the boundary condition $R_0 = 1$ is fulfilled.)

The recurrence relations (34,35) for $Q_m^{(a,b)}$'s are of a more complicated nature. So, the second order differential equations satisfied by the corresponding generating functions $Q^{(a,b)}(\zeta)$ are more complicated than the hypergeometric equation. (These equations have four singular points; we have derived them but we do not feel that they are *in situ* here.) Unfortunately, we have not been able to solve these equations.

On the other hand, we are mostly interested in the low-energy regime $s \rightarrow 0$. There one can simplify the recurrence relations and change over to differential equations. Indeed, in the low-energy limit the high order diagrams matter, so that we shall restrict ourselves to the parameter region

$$s \rightarrow 0, m \rightarrow \infty \text{ while } sm \text{ finite.} \tag{37}$$

An inspection of the formula (36), shows that in the limit (37)

$$R(z) = -\frac{2}{\ln(-is)} K_0(z), \tag{38}$$

where we have introduced the variable

$$z = \sqrt{-2ims}. \tag{39}$$

[For large m we can replace $[t/(t+1)]^m$ by $\exp(-m/t)$ in (36) and the remaining integral, upon rescaling the integration variable, gives the MacDonal function.]

An alternative way to obtain this approximate solution is to pass to the limit of large m in (28)²⁵. Expanding $R_{m\pm 1}$ and neglecting the terms vanishing in the limit (37), one finds

$$m^2 \frac{d^2 R_m}{dm^2} + m \frac{dR_m}{dm} + \frac{i}{2} sm R_m = 0.$$

Making the substitution (39) one arrives at the modified Bessel equation

$$\frac{d^2 R}{dz^2} + \frac{1}{z} \frac{dR}{dz} - R = 0.$$

A general solution to this equation is $R(z) = AK_0(z) + BI_0(z)$. The coefficient B must vanish for the function $I_0(z)$ diverges at infinity. The coefficient A is to be determined by the boundary condition (29). Since the MacDonald function diverges as $z \rightarrow 0$, we must recall that the variable z is discrete. There is a $z_{\min} = \sqrt{-2is}$, so that $A = 1/K_0(z_{\min}) \simeq -2/\ln(-is)$, in agreement with (38) within the leading logarithmic accuracy. (Within this approximation one must generally neglect C -numbers as compared to the \log 's. Yet we are keeping the imaginary part of the \log 's. Alternatively, the imaginary parts can be restored at the end of the calculation by a simple analytic continuation, i.e. demanding that the Green function be retarded.)

Let us now determine the quantities $Q_m^{(a,b)}$ in the limit (37). The recurrence relations (34) and (35) become identical for large m and reduce to

$$2m^2 \frac{d^2 Q_m^{(a,b)}}{dm^2} + 4m \frac{dQ_m^{(a,b)}}{dm} + \left(\frac{1}{2} - i\kappa + ism \right) Q_m^{(a,b)} = R_m \quad (40)$$

Since the summation over m in formula (33) is now to be changed to the integration over z [according to $\sum_{m=0(1)}^{\infty} \rightarrow (i/s) \int_0^{\infty} z dz$], the Green function is determined by the sum $Q = Q^{(a)} + Q^{(b)}$. The equation for the latter follows from (39) and (40):

$$z^2 \frac{d^2 Q}{dz^2} + 3z \frac{dQ}{dz} - (z^2 + 2i\kappa - 1)Q(z) = 4R(z). \quad (41)$$

Rewriting the equation (41) in the form

$$\frac{d}{dz} \left[z \frac{d(zQ)}{dz} \right] - \left(z + \frac{2i\kappa}{z} \right) (zQ) = 4R(z), \quad (42)$$

we identify it as an inhomogeneous modified Bessel equation for the function $zQ(z)$.

Equations of this type are usually solved by means of the Lebedev–Kontorovich transformation²⁶. We employ the Lebedev–Kontorovich transformation in the form

$$\hat{Q}(\tau) = \int_0^{\infty} dz K_{i\tau}(z) Q(z), \quad (43)$$

where $K_{i\tau}(z)$ is the MacDonald function of a purely imaginary index. The transformation inverse to (43) is

$$Q(z) = \frac{2}{\pi^2 z} \int_0^{\infty} d\tau \tau \sinh(\pi\tau) K_{i\tau}(z) \hat{Q}(\tau). \quad (44)$$

Applying the integral operator (43) to the equation (42), re-grouping the terms and then using the inverse transformation (44), we find the solution in the form

$$Q(\kappa, z) = \frac{2}{\pi^2 z} \int_0^\infty d\tau \tau \sinh(\pi\tau) \frac{K_{i\tau}(z)}{\tau^2 + 2i\kappa} \int_0^\infty d\xi K_{i\tau}(\xi) 4R(\xi) , \quad (45)$$

where we have restored the dependence of the function Q on the parameter κ .

At this point we notice that (45) is normalized as

$$\int_{-\infty}^{\infty} \frac{d\kappa}{2\pi} Q(\kappa, z) = 2R(z) . \quad (46)$$

According to the definition (32), the normalization (46) corresponds to the boundary conditions (20).

Substituting the asymptotic form (38) into (45) and looking the ξ -integral up in Ref. 27, we finally obtain

$$Q(\kappa, z) = -\frac{8}{z \ln(-is)} \int_0^\infty d\tau \tau \tanh\left(\frac{\pi\tau}{2}\right) \frac{K_{i\tau}(z)}{\tau^2 + 2i\kappa} . \quad (47)$$

C. Calculation of Green's function

It is now instructive to Fourier transform the Green function (33) back to the coordinate space:

$$G_R^+(y, s) = \frac{1}{vs} \int_0^\infty dz z R(z) Q(y, z) . \quad (48)$$

The function Q in the space domain is of the form

$$Q(y, z) = -\frac{4}{z \ln(-is)} \int_0^\infty d\tau \tau \tanh\left(\frac{\pi\tau}{2}\right) K_{i\tau}(z) e^{-\frac{\tau^2}{2}y} . \quad (49)$$

The z -integration is performed in Appendix A. The final result for the Green function is

$$G_R^+(y, s) = \frac{4}{vs \ln^2(-is)} F(y) , \quad (50)$$

where the function $F(y)$ is defined by

$$F(y) = 2 \int_0^\infty dx x \tanh x (1 - \tanh^2 x) e^{-\frac{2}{\pi^2}yx^2} . \quad (51)$$

The limiting behavior of the function $F(y)$ is

$$F(y) = \begin{cases} 1 - \frac{1}{2}y + O(y^2), & \text{for } y \ll 1 \\ 2\pi^2 \left(\frac{\pi}{2y}\right)^{3/2} + O(y^{5/2}), & \text{for } y \gg 1 \end{cases} \quad (52)$$

The function $F(y)$ is plotted in Fig.6. Notice that the correct density of states (Dyson singularity) is reproduced as $y \rightarrow 0$:

$$\rho(s) = -\frac{1}{\pi} \text{Im}G_R^+(y \rightarrow 0, s) \simeq \frac{8\pi\rho_0}{s \ln^3(1/s)}, \quad (53)$$

where $\rho_0 = 1/(2\pi v)$ is the bare density of states (in the chiral branches of the fermion spectrum).

V. BOUNDARY EFFECTS

In this section we study the influence of boundaries onto single-particle properties of the random mass Dirac problem. This study is largely inspired by the investigation of the boundary effects for the standard one-dimensional localization by AP¹⁵. AP succeeded in calculating the whole distribution function of the local density of states (for an infinite system as well as in the presence of boundaries). Technically, this success was due to a factorization of the high-order correlation functions into combinations of known Beresinskii blocks^{15,11}. Unfortunately, for the random mass Dirac problem such a factorization does not occur. So, at the time being we do not know the distribution functions. On the other hand, as we shall see shortly, already the simplest quantity – the local density of states – displays quite an interesting boundary behavior for the Dirac problem.

A. Modification of the diagram technique

We consider a semi-infinite sample ($x > 0$), i.e. we assume an infinite potential wall to be situated at the origin (the electrons can not leave the sample). As a result of the total reflection from the boundary the single-particle eigenfunctions of the Hamiltonian without the disorder potential change over from the plane waves to the standing waves:

$$\frac{1}{\sqrt{L}} e^{ipx} \rightarrow \sqrt{\frac{2}{L}} \sin(px).$$

The bare Green function therefore takes the form

$$\begin{aligned} G_{\text{open}}^{0+}(x', x; \epsilon) &= \frac{1}{2} \left[G^{0+}(x - x', \epsilon) + G^{0+}(x' - x, \epsilon) \right. \\ &\quad \left. - G^{0+}(x + x', \epsilon) - G^{0+}(-x - x', \epsilon) \right] \\ &= G^{0+}(x - x', \epsilon) - G^{0+}(x + x', \epsilon). \end{aligned} \quad (54)$$

The last equality follows from the fact that $G^{0+}(-x) = G^{0+}(x)$ for the translationally invariant system, Eq.(18).

Let us take a closer look at the second term in the expression (54) which is due to the presence of the boundary. This term can be written as

$$-G^{0+}(x+x', \epsilon) = \frac{i}{v} e^{i(k_F + \epsilon/v)(x+x')} = \{-1\} \left\{ \sqrt{-\frac{i}{v}} e^{i(k_F + \epsilon/v)x'} \right\} \left\{ \sqrt{-\frac{i}{v}} e^{i(k_F + \epsilon/v)x} \right\}. \quad (55)$$

In terms of the Berezinskii diagrams this term can be represented as shown in Fig.7. The second and the third factors in curly brackets in the expression (55) correspond to the external vertices x' and x respectively, while the $\{-1\}$ factor must be attached to the new element of the diagram technique – the ‘boundary vertex’ at $x = 0$. Physically this vertex can be interpreted as a total reflection from the boundary. (Any phase factor, like $-1 = \exp(i\pi)$, corresponds to a shift of the position of the boundary and can be omitted.)

Thus, in the presence of a totally reflective boundary the Berezinskii diagram technique is modified by adding the boundary vertex: Fig.7.

B. Density of states

The density of states at the point x is given by the general formula (23). We must therefore consider the one-loop diagrams: the electron line starting at the point x returns, after undergoing scattering processes and reflections from the boundary, to the same point x . An example of a diagram involving the boundary scattering is shown in Fig.8. Notice that the boundary vertex changes the number of electron lines by $\Delta g = 2$. Therefore, in addition to the end point configurations Fig.2(a,b) at work for the infinite system, the configurations Fig.2(c,d) are also allowed.

The diagram Fig.7, in combination with the bare Green function, determines the density of states in the pure system:

$$\rho_0(x, \epsilon) = \rho_0 \left\{ 1 - \cos \left[2 \left(k_F + \frac{\epsilon}{v} \right) x \right] \right\}. \quad (56)$$

The $2k_F$ -oscillation of the density of states is due to the fact that the single-electron eigenfunctions are standing waves and is not of great interest. We can get rid of this oscillation by adopting the following averaging procedure

$$\rho(x, \epsilon) \rightarrow \bar{\rho}_\Delta(x, \epsilon) = \frac{1}{2\Delta} \int_{-\Delta}^{\Delta} dy \rho(x+y, \epsilon). \quad (57)$$

Such averaging over the spatial coordinate has also been discussed by AP¹⁵. The parameter Δ in Eq.(57) is chosen in such a way that

$$\frac{1}{k_F} \ll \Delta \ll \min \left(l, \frac{v}{\epsilon} \right). \quad (58)$$

With this choice of Δ the $2k_F$ oscillation in (56) averages away so that

$$\bar{\rho}_\Delta(x, \epsilon) = \rho_0 \left[1 + O \left(\frac{1}{k_F \Delta} \right) \right]. \quad (59)$$

It is important to notice that all the diagrams with the end point configurations Fig.2(c,d), however complicated, have an additional rapidly oscillating factor $\exp(\pm 2k_F x)$

as compared to the diagrams with end point configurations Fig.2(a,b). Upon averaging (57), the former diagrams acquire [as (59)] a small factor of the order of $\sim 1/(k_F\Delta)$. We shall therefore neglect these diagrams. (We also observe that the remaining diagrams do not depend on Δ , so we drop this subscript in what follows.)

Defining the Berezinskii blocks in full analogy to the translationally invariant case, we rewrite the expression (23) for the density of states in the form

$$\bar{\rho}(x, \epsilon)/\rho_0 = 1 + 2\text{Re} \sum_{m=1}^{\infty} \tilde{R}_m(x)R_m(x) . \quad (60)$$

[The mirror imaged diagrams like Fig.5 remain such even if the boundary vertex is involved (with respect to the horizontal axes). Hence the factor of 2 in (60).]

The right-hand-side blocks $R_m(x)$ are not influenced by the boundary at all. Hence they are identical to those for the translationally invariant system (Section IV). As to the left-hand-side blocks $\tilde{R}_m(x)$, the presence of the boundary vertex on the left can not alter the process of constructing this diagrams by adding impurity vertices from the right. Hence \tilde{R}_m 's satisfy the same differential recurrence relation as they do for the infinite system: Eq.(24). What is new in the open boundary case is that a boundary condition at $x = 0$ comes into play. Indeed, consider the quantity $\tilde{R}_m(x \rightarrow 0)$. Tending x to zero means squeezing the diagrams $\tilde{R}_m(x)$ so that only $2m$ boundary vertices (and no impurity vertices) contribute to $\tilde{R}_m(0)$. Hence the boundary condition

$$\tilde{R}_m(x = 0) = 1 \quad \text{for all } m . \quad (61)$$

Next we define [c.f. 27]

$$\begin{cases} R_m(x) = (-1)^m e^{i\frac{4\epsilon}{v}mx} R_m , \\ \tilde{R}_m(x) = (-1)^m e^{-i\frac{4\epsilon}{v}mx} L_m(y) . \end{cases} \quad (62)$$

The Berezinskii blocks R_m are defined in Section IV [Eq.(36)], while the blocks $L_m(y)$ satisfy

$$\begin{cases} \frac{dL_m}{dy} = m \{isL_m - [4mL_m - (2m-1)L_{m-1} - (2m+1)L_{m+1}]\} , \\ L_m(y = 0) = 1 , \end{cases} \quad (63)$$

Equation (60) now reads

$$\frac{\bar{\rho}(y, s)}{\rho_0} = 1 + 2\text{Re} \sum_{m=1}^{\infty} L_m(y)R_m . \quad (64)$$

Equation (63) [in combination with Eq.(64) and Eq.(36)] determines, in principle, the exact density of states. Unfortunately, we failed to obtain the solution to the differential recurrence relation (63) in a closed form. [Upon making the Laplace transform with respect to y , one can reduce (63) to an algebraic recurrence relation. That is, however, not any simpler than the relations (34,35) for $Q^{(a,b)}$.] On the other hand, we are primarily interested in the low-energy ($s \ll 1$) behavior of the density of states. So, as in Section IV, it is sufficient to consider the limit (37). For large m , the relation (63) reduces to the differential equation

$$\frac{2}{z} \frac{\partial L}{\partial y} = \frac{\partial}{\partial z} \left(z \frac{\partial L}{\partial z} \right) - zL, \quad (65)$$

(We recall that $z = \sqrt{-2ims}$.) Since the operator on the right-hand-side of (65) is the operator defining the modified Bessel equation, we again (as in Section IV) use the Lebedev–Kontorovich transformation²⁶. It is convenient to define

$$\begin{cases} F(y, \tau) = \int_0^\infty \frac{dz}{z} K_{i\tau}(z) L(y, z), \\ L(y, z) = \frac{2}{\pi^2} \int_0^\infty d\tau \tau \sinh(\pi\tau) K_{i\tau}(z) F(y, \tau). \end{cases} \quad (66)$$

Applying the transformation (66) to the equation (65) we find that the function $F(y, \tau)$ satisfies the equation

$$\frac{\partial F(y, \tau)}{\partial y} = -\frac{1}{2} \tau^2 F(y, \tau). \quad (67)$$

The solution of this equation is

$$F(y, \tau) = F_0(\tau) e^{-y\tau^2/2}. \quad (68)$$

The function $F_0(\tau) = F(0, \tau)$ is determined by the boundary condition (63)

$$F_0(\tau) = \int_0^\infty \frac{dz}{q} K_{i\tau}(z) L(0, z) = \frac{\pi}{2\tau \sinh(\pi\tau/2)}. \quad (69)$$

Combining (69,68), and (66) we find the function $L(y, z)$ in the form

$$L(y, z) = \frac{2}{\pi} \int_0^\infty d\tau \cosh(\pi\tau/2) e^{-y\tau^2/2} K_{i\tau}(z). \quad (70)$$

This equation can be re-written in a simpler way as

$$L(y, z) = \sqrt{\frac{2}{\pi y}} \int_0^\infty dx \cos(z \sinh x) \exp\left(-\frac{x^2}{2y}\right). \quad (71)$$

Substituting this expression into the formula (64), replacing the sum over m by the integral over q and using the asymptotic expression (38) for R_m 's, we find the density of states in the form

$$\bar{\rho}(y, s) = \frac{2\pi\rho_0}{s \ln^2(1/s)} f(y). \quad (72)$$

The function $f(y)$ is given by

$$f(y) = \sqrt{\frac{2}{\pi y}} \int_0^\infty \frac{dx}{\cosh^2 x} (1 - x \tanh x) \exp\left(-\frac{x^2}{2y}\right). \quad (73)$$

It is plotted in Fig.9. The limiting values of the function f are

$$f(y) = \begin{cases} 1 + O(y), & \text{for } y \ll 1 \\ \left(\frac{2}{\pi y}\right)^{1/2} + O(y^{3/2}), & \text{for } y \gg 1 \end{cases} \quad (74)$$

As follows from (72), close to the boundary the local density of states turns out to be logarithmically enhanced as compared to the bulk one [c.f. (53)]

$$\bar{\rho}(y=0, s) = \frac{2\pi\rho_0}{s \ln^2(1/s)} \quad (75)$$

(see also Appendix B). Away from the boundary this enhancement is exhausted, for the function $\bar{\rho}(y, s)$ decays as ($y \gg 1$):

$$\bar{\rho}(y, s) \simeq \frac{\sqrt{8\pi}\rho_0}{s \ln^2(1/s)} \frac{1}{\sqrt{y}} \quad (76)$$

It crosses over to the bulk value (53) at the distances y of the order of $\ln^2(1/s) \sim L_s$. Thus the boundary influences the local density of states on the scale of the order of the correlation length. A similar conclusion has been reached by AP on the basis of the boundary density of states distribution function¹⁵ (we refer to the case when the excitations can not leave the sample). In our case, the difference with the standard localization problem is that perturbations caused by the boundary decay into the bulk on the scale L_s , not λ_s , and that they follow a power law, not an exponential decay.

C. Density of states by renormalization group

In the Introduction we have referred to real-space renormalization group (RG) calculations for random spin models. It is worth to investigate how this alternative approach works for calculating the local density of states close to the boundary. We use the real space version of the RG, introduced by Dasgupta and Ma³ and extended by Fisher⁴, to cope with disordered exchange constants in an Heisenberg chain. In fact, the random Heisenberg model in the anisotropic XY limit and at zero magnetization is equivalent to a model of spinless fermions with random nearest-neighbor hopping integrals at half-filling. As we said, the random hopping has a particle-hole symmetry at half-filling, which prevents the generation of forward scattering processes. Therefore, this model is exactly equivalent to the random backscattering model. Moreover, it was shown⁴ that the spin anisotropy is not a relevant parameter, and that in the whole range $0 \leq J_z \leq J_x = J_y$ the physical behavior is unchanged, including also the exponents of the power-law decaying correlation functions. Hence, we are going to consider the spin-isotropic case.

The RG procedure consists in successive eliminations of pairs of spins, which are coupled more strongly than the others. The cut-off energy Ω , which is rescaled downwards, is simply the largest exchange coupling $\Omega = \text{Max}(J)$ at a given stage of the RG process. Once a pair of spins is decimated, an effective exchange is generated between the two spins adjacent to the decimated bond. The probability $Q(y, \Gamma)$ that a bond of length y will be decimated at the scale $\Omega = \Omega_0 e^{-\Gamma}$ has been calculated in Ref. 4 (Ω_0 being the cut-off energy at the start of the RG process).

Let us consider a semi-infinite chain. The probability $n(x, \Gamma)$ that the spin at site $x \in [0, \infty]$ is still free at the scale Ω satisfies the differential equation:

$$\frac{d \ln n(x, \Gamma)}{d\Gamma} = - \int_0^x dy Q(y, \Gamma) - \int_0^\infty dy Q(y, \Gamma). \quad (77)$$

The two integrals on the right-hand-side imply that the spin at x gets bound to a spin at its left or its right. From the RG equations, one finds that $Q(y, \Gamma)$ at $\Gamma \gg 1$ is given by the inverse Laplace transform^{4,28}

$$\begin{aligned} Q(y, \Gamma) &= \int_{c-i\infty}^{c+i\infty} \frac{dz}{2\pi i} \frac{\sqrt{z}}{\sinh(\sqrt{z}\Gamma)} e^{zy/2} \\ &= \frac{\pi^2}{\Gamma^3} \sum_{m=1}^{\infty} (-1)^{m+1} m^2 e^{-\pi^2 m^2 y / (2\Gamma^2)}. \end{aligned} \quad (78)$$

From this equation one derives that

$$\int_0^\infty dy Q(y, \Gamma) = \frac{1}{\Gamma},$$

and, for $1 \ll x \ll \Gamma^2$,

$$\int_1^\Gamma d\Gamma' \int_0^x dy Q(y, \Gamma') \simeq \frac{1}{2} \ln \left(\frac{\pi^2 x}{2} \right).$$

The limiting expressions of $n(x, \Gamma)$ can easily be obtained from the above equations:

$$n(x, \Gamma) \simeq \begin{cases} \frac{1}{\Gamma^2} & \text{for } x \gg \Gamma^2 \\ \frac{1}{\Gamma \sqrt{x}} & \text{for } 1 \ll x \ll \Gamma^2 \\ \frac{1}{\Gamma} & \text{for } x \ll 1 \end{cases}$$

In the fermion language, $n(x, \Gamma)$ is proportional to the local density of states $\rho(x, \epsilon)$ integrated up to the energy $\epsilon = \Omega_0 e^{-\Gamma}$. We finally obtain

$$\rho(x, \epsilon) \sim \begin{cases} \frac{1}{|\epsilon| \ln^3(1/|\epsilon|)} & \text{for } x \gg L_\epsilon \\ \frac{1}{\sqrt{x} |\epsilon| \ln^2(1/|\epsilon|)} & \text{for } 1 \ll x \ll L_\epsilon \\ \frac{1}{|\epsilon| \ln^2(1/|\epsilon|)} & \text{for } x \sim 1 \end{cases}$$

where the cross-over length $L_\epsilon = 2 \ln^2(\epsilon) / \pi^2$. The resulting density of states is therefore in perfect agreement with the previous calculation. An important observation is that from the RG analysis it comes out quite naturally that the relevant correlation length in this problem is L_ϵ . This is one of the main achievements of this approach, as we are going to discuss in the following section. Before concluding this section, it is worthwhile to briefly discuss the enhancement of the local density of states close to a boundary in the light of the

RG approach. The RG provides a quite simple picture of the ground state of the random Heisenberg model, in terms of the so-called ‘random singlet state’⁴. With this we intend a state where each spin is coupled into a singlet with another spin, and the longer the distance between the two coupled spins the lower the excitation energy of the singlet. Hence, it is more or less obvious that a spin close to a boundary has less probability to get coupled to another spin, which explains the enhancement of the density of states at low energy.

VI. DISCUSSION AND CONCLUSIONS

To summarize, in this paper we have investigated the single-particle Green function and the local density of states in the presence of boundaries for the random mass Dirac problem. Let us discuss these findings in reverse.

For the density of states of the random mass Dirac fermions is strongly energy dependent (Dyson singularity), it is not a surprise that the presence of the boundary is essential. It is perhaps less obvious that the density of states close to the boundary is strongly enhanced as compared to the bulk one²⁹

$$\bar{\rho}(x=0, s)/\rho(s) \simeq \frac{1}{4} \ln(1/s). \quad (79)$$

Regarding the spin systems, this result is relevant for the situation when one considers the effect of especially strong impurities (like lattice defects) in an already doped sample. Indeed, the Dyson singularity itself readily yields peculiar thermodynamic properties^{17,18}. For example, the linear magnetic susceptibility diverges as $\chi(T) \sim 1/T \ln^2(1/T)$ ³⁰. Heeding (79), one expects (larger) contributions of the order of

$$\chi(T) \sim 1/T \ln(1/T)$$

to the magnetic susceptibility due to strong impurities and, of course, sample boundaries (the latter are especially important for powder samples on which most of the experiments are presently being conducted²¹).

According to the result (50), the single-particle Green function behaves as

$$G^+(x, s) \sim \frac{\rho_0}{s \ln^2(-is)} \left(\frac{1}{x}\right)^{3/2}, \quad (80)$$

in the region $l \ll x \ll L_s$. (In the region $x \gg L_s$ we expect the Green function to cross over to a standard exponential decay.) It is worth noting that the Green function (80) has a large prefactor. Therefore it is actually larger than the bare Green function $G^{(0+)} \sim \rho_0$ on the whole scale $l \ll x \ll L_s$. The conclusion is that not only the density of states is large (that is not surprising for the zero-modes are packed around zero energy), but also the correlations are strong. In fact, the one-particle correlations in the disordered system are stronger than those in a pure system (without the gap). This is only true below a certain energy scale, which vanishes with the impurity concentration.

The length scale $L_s \simeq l \ln^2 s$, below which (80) is valid, can be inferred from the analysis of the boundary effects. The same scaling relation of the length x versus the energy s , $x \sim l \ln^2(s)$, was found in Ref. 12 by means of a replica method analysis of the Dirac fermion

model, and also was derived by the RG investigation of the random Heisenberg model in Ref. 4. Surprisingly, it differs from the scaling relation that the energy dependence of the localization length would suggest, namely $x \sim \lambda(s) = l |\ln s|$. This is an evident signature that the typical behavior differs from the average behavior, the difference becoming large as $s \rightarrow 0$. In other words, some physical quantities are dominated by very rare events.

Notice that L_s does not come out in any simple way from our asymptotic calculation of the Green function. The likely reason is that, once we solve the recurrence relations for the Berezinskii blocks under the restriction (37), we are implicitly assuming that $L_s \gg x$. This denies the access to the region $x \gg L_s$ where the Green function decays exponentially. This issue ought to be further studied¹⁶. In fact, in the case when we knew the $x \gg L_s$ asymptotics, that is for the density of states in the presence of a boundary, we have been able to identify L_s .

As we mentioned in the Introduction, also the RG method gives access to the correlation functions, although at equal times. In particular, the equal-time spin-spin correlation function is known to decay at large distances as⁴

$$\langle S^i(x) S^i(0) \rangle \sim \frac{1}{x^2},$$

($i = x, y, z$). One can show²⁸ that also the equal-time Green function in the equivalent random hopping tight-binding model decays as $1/x^2$. This result is, in fact, compatible with (80). Indeed, (80) is only valid for $x \ll L_s$, or, equivalently, for $s \ll s(x) = \exp(-\sqrt{x/l})$. Therefore, neglecting exponentially decaying terms, we find

$$G^+(t=0, x) \sim \int_0^{s(x)} ds G^+(x, s) \sim \frac{\rho_0}{x^{3/2}} \int_0^{s(x)} \frac{ds}{s \ln^2 s} \sim \frac{1}{x^2}, \quad (81)$$

in agreement with the RG results. Hence our results not only reproduce the equal-time behavior of the correlation functions found by RG, but also allow us to determine their energy dependence.

According to GM¹⁴, the two-particle correlations follow the same pattern as (80). The fact that the disorder actually enhances correlations (at low energy scale) throws the light onto the experimental findings of an antiferromagnetizing ordering in the spin-Peierls compounds building up upon doping¹. Indeed, the system without the spin-phonon interactions is known to be unstable with respect to the antiferromagnetic ordering. In a pure system, however, the latter is prevented by the spin gap. The doping effectively creates states in the gap and induces correlations that are even stronger than those in a pure system without the spin gap. Hence the antiferromagnetism is promoted by doping. This matter, though, is to be investigated in more detail, especially with respect to the energy scales involved (we expect the relevant scale be associated with the fluctuations of the density-density correlator)^{16,31}.

To conclude, in this paper we have analyzed single-particle properties of the random mass Dirac problem in some detail. The lack of knowledge of the distribution functions (for the density of states, etc.), however, calls upon further exploration of the problem.

VII. ACKNOWLEDGEMENTS

We are thankful to Y. Chen, S. Gogolina, and R. Mèlin for interesting and helpful discussions. M.F. was supported by INFN, under project HTCS. A.O.G. was supported by the EPSRC of the United Kingdom. M.S. was supported by the Gottlieb Daimler- und Karl Benz- Stiftung.

VIII. APPENDIX A

In order to evaluate the integrals in (48, 49), which read

$$F(y) = \int_0^\infty dz K_0(z) \int_0^\infty d\tau \tau \tanh\left(\frac{\pi\tau}{2}\right) K_{i\tau}(z) e^{-\frac{\tau^2}{2}y}, \quad (82)$$

we make use of Nicholson's integral representation of the product of MacDonald functions³²

$$K_0(z)K_{i\tau}(z) = 2 \int_0^\infty dt \cos(\tau t) K_{i\tau}(2z \cosh t). \quad (83)$$

Upon substituting (83) into (82) one observes that the z -integral and the t -integral, if taken in succession, are the table ones²⁷. Hence (51).

IX. APPENDIX B

Exactly at the sample boundary the local density of states can be explicitly evaluated. Indeed, owing to the boundary condition (61), the formula (60) for the density of states simplifies so that the summation over the number of lines is easily performed [c.f. (36)]:

$$\bar{\rho}(x=0, \epsilon)/\rho_0 = 1 + 2\text{Re} \sum_{m=1}^{\infty} R_m = -1 + 2\text{Re} \left\{ \frac{2e^{is/4}}{K_0(-is/4)} \int_0^\infty dt \sqrt{\frac{t+1}{t}} e^{ist/2} \right\}.$$

The above integral is a table one²⁷, so that we finally obtain

$$\bar{\rho}(x=0, \epsilon)/\rho_0 = \text{Re} \left\{ \frac{K_1(-is/4)}{K_0(-is/4)} \right\} \quad (84)$$

[the $s \rightarrow 0$ limit of this formula is in agreement with Eq.(72)].

REFERENCES

- ¹ For a review see J.P. Boucher and L.P. Regnault, *J. Phys. I France* **6**, 1939 (1996).
- ² For a review see E. Dagotto and T.M. Rice, *Science* **271**, 618 (1996).
- ³ C. Dasgupta and S.K. Ma, *Phys. Rev. B* **22**, 1305 (1980).
- ⁴ D.S. Fisher, *Phys. Rev. B* **50**, 3799 (1994); *Phys. Rev. B* **51**, 6411 (1995).
- ⁵ R.A. Hyman, K. Yang, R.N. Bhatt, and S.M. Girvin, *Phys. Rev. Lett.* **76**, 839 (1996).
- ⁶ A.A. Ovchinnikov and N.S. Erikhman, *Zh. Eksp. Teor. Fiz.* **73**, 650 (1977) [*Sov. Phys. JETP* **46**, 340 (1977)].
- ⁷ The case of a random telegraph signal mass has recently been solved by A. Comtet, J. Desbois, and C. Monthus, *Ann. Phys.* **239**, 312 (1995). The low-energy asymptotics of the density of states coincides with (1). This strongly suggests that the Gaussian distribution of the mass is genuine and can be used for describing the low-energy fixed point.
- ⁸ F.J. Dyson, *Phys. Rev.* **92**, 1331 (1953).
- ⁹ M. Weissman and N.V. Cohan, *J. Phys. C* **8**, 145 (1975).
- ¹⁰ D.J. Thouless, *J. Phys. C* **5**, 77 (1972). See also G. Theodorou and M.H. Cohen, *Phys. Rev. B* **13**, 4579 (1976); and T.P. Eggarter and R. Riedinger, *Phys. Rev. B* **18**, 569 (1978).
- ¹¹ V.L. Berezinskii, *Zh. Eksp. Teor. Fiz.* **65**, 1251 (1973) [*Sov. Phys. JETP*, **38** (3), 620 (1974)]. See also A.A. Gogolin, V.I. Mel'nikov, and E.I. Rashba, *Zh. Eksp. Teor. Fiz.* **69**, 327 (1975) [*Sov. Phys. JETP* **42**, 168 (1976)].
- ¹² J.P. Bouchaud, A. Comtet, A. Gorges, and P. Le Doussal, *Ann. Phys.* **201**, 285 (1990).
- ¹³ D.G. Shelton and A.M. Tsvelik, Report No. cond-mat/9704115.
- ¹⁴ A.A. Gogolin and V. I. Mel'nikov, *Zh. Eksp. Teor. Fiz.* **73**, 706 (1977) [*Sov. Phys. JETP* **46**(2), 369 (1977)]. See also A.A. Gogolin, *Phys. Rep.* **86**, 1 (1982).
- ¹⁵ B.L. Al'tshuler and V.N. Prigodin, *Zh. Eksp. Teor. Fiz.* **95**, 348 (1989) [*Sov. Phys. JETP* **68**(1), 198 (1989)].
- ¹⁶ M. Steiner, M. Fabrizio, and A.O. Gogolin (unpublished).
- ¹⁷ M. Fabrizio and R. Melin, *Phys. Rev. Lett.* **78**, 3382 (1997).
- ¹⁸ A.O. Gogolin, A.A. Nersesyan, A.T. Tsvelik, and Lu Yu (unpublished).
- ¹⁹ D.G. Shelton, A.A. Nersesyan and A.M. Tsvelik, *Phys. Rev. B* **53**, 8521 (1996).
- ²⁰ More precisely, the Dirac model occurs in the total spin spin sector, while there also are two massive Majorana fermions in the 'spin-flavor' sector: see discussion in Ref. 19.
- ²¹ The *Sr* doping has been achieved in, e.g., M. Tanako, *Nature* **377**, 41 (1995). Very recently, *Zn* doping (which substituted *Cu* in *SrCu₂O₃* spin-ladder systems) also become possible: M. Azuma, Y. Fujishiro, M. Takano, M. Nohara, and H. Takagi, *Phys. Rev. B* **55**, R8658 (1997).
- ²² A more formal way to see this is to track the spatial dependence of the average charge phase field (which effectively takes care of the site numbering) in the definition of the staggered magnetization $\vec{n}(x)$ ¹⁸.
- ²³ This does not lead to 'over-counting'. Indeed, after averaging over the disorder, one finds contributions to the Green function given as unlimited integrals over the spatial coordinates. Each of these contributions splits into a sum of terms with the spatial integration taken over a given *x*-ordered domain. These correspond to different arrangements of the 'interaction' vertices so that each of them is represented by an unique diagram.
- ²⁴ The factor 1/2 in the Fig.1 vertex contribution follows from the absence of the forward

scattering. A right-moving electron follows the left-moving electron (or *vice versa*). Hence $\theta(x=0) = 1/2$ from (17) is at work. See Ref. 11 for a detailed discussion.

- ²⁵ A.A. Gogolin, Zh. Eksp. Teor. Fiz. **77**, 1649 (1979) [Sov. Phys. JETP **50**(4), 827 (1979)].
- ²⁶ V.A. Ditkin and A.P. Prudnikov, *Integral Transform and Operational Calculus*, Pergamon, London (1965).
- ²⁷ I.S. Gradshteyn and I.M. Ryzhik, *Table of Integrals, Series, and Products*, edited by A. Jeffrey, Academic Press Ltd., London (1994).
- ²⁸ M. Fabrizio and R. Mélin, Report No. cond-mat/9703102.
- ²⁹ This must be contrasted with the recently debated situation in (pure) repulsive Luttinger liquids, where the boundary tends to suppress the local density of states. See A.O. Gogolin and M. Fabrizio, Phys. Rev. Lett. (1997) (in press) and references therein.
- ³⁰ This particular result has already been known to GM¹⁴. See also L.N. Bulaevskii, R.B. Lyubovskii, and I.F. Shchegolev, Pis'ma Zh. Eksp. Teor. Fiz. **16**, 42 (1972) [Sov. Phys. JETP Lett. **16**, 29 (1972)].
- ³¹ Theoretical outlook for the spin-ladder systems, where an antiferromagnetic tendency upon doping has recently been discovered²¹, is less clear. The reason is that in these systems, unlike the spin-Peierls systems¹⁷, the staggered magnetization is not directly related to the density-density correlation function of the Dirac fermions, but it is a more complex object¹⁹.
- ³² G.N. Watson, *A Treatise on the Theory of the Bessel functions*, Cambridge University Press (1966).

FIGURES

FIG. 1. The elementary vertices of the Berezinskii diagram technique contributing the factors (a) $-1/(2l)$, (b) $-1/l$, (c) $-(1/l) \exp[-i(\epsilon/v)x]$, (d) $-(1/l) \exp[+i(\epsilon/v)x]$.

FIG. 2. The configurations of the electron line end points for the single-particle Green function.

FIG. 3. This figure illustrates the definition of Berezinskii blocks for the diagrams with end point configuration shown in Fig. 2(a).

FIG. 4. The process of joining the elementary vertices for deriving the recurrence relation for the right-hand-side blocks $\tilde{R}_m(x)$.

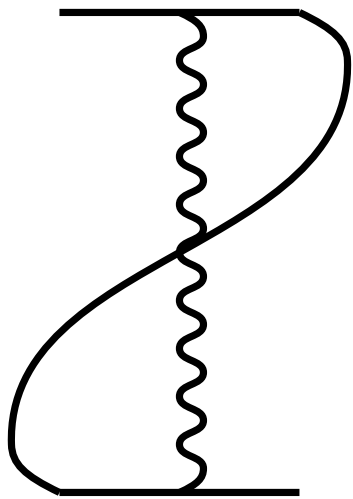
FIG. 5. Two fourth order mirror imaged (coinciding end points) diagrams contributing to the Green function.

FIG. 6. The plot of the function $F(y)$ determining the spatial decay of the single-particle Green function.

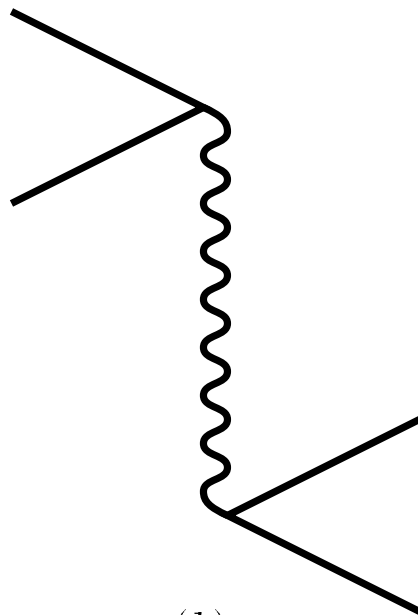
FIG. 7. The new element of the diagram technique in the presence of the boundary – the boundary vertex.

FIG. 8. An example of a diagram involving the boundary scattering.

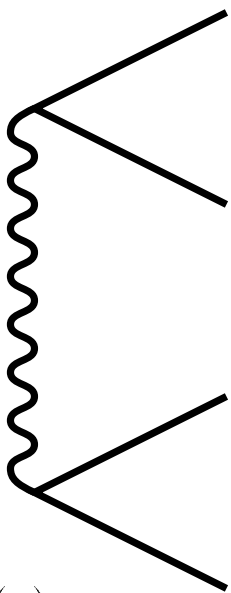
FIG. 9. The plot of the function $f(y)$ determining the spatial decay of the local density of states away from the boundary.



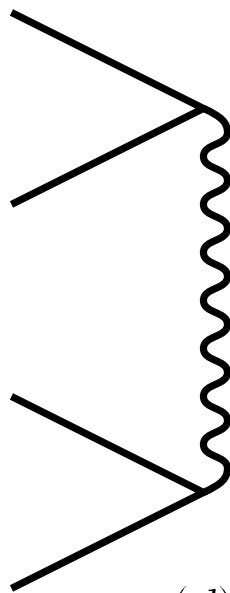
(a)



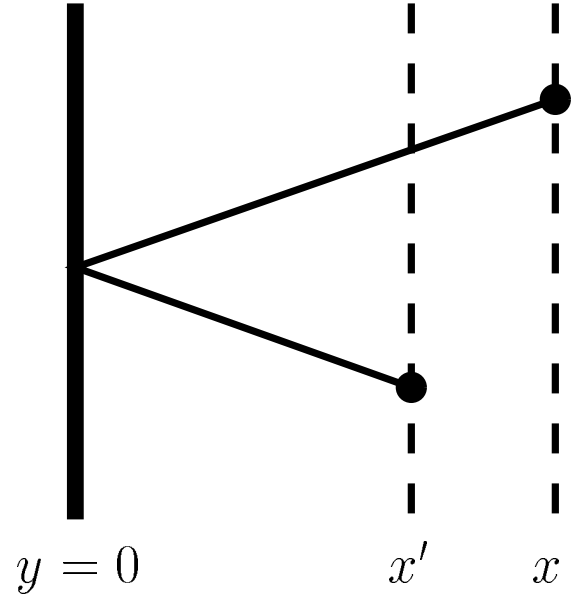
(b)

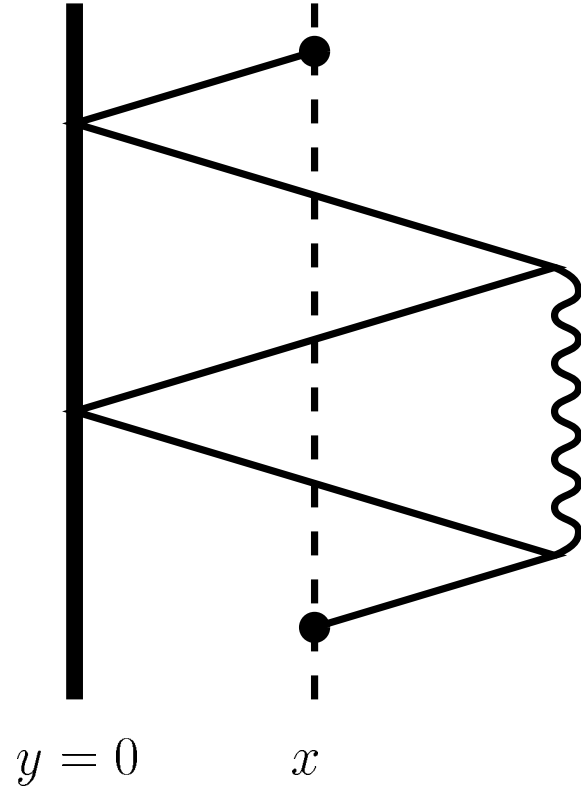


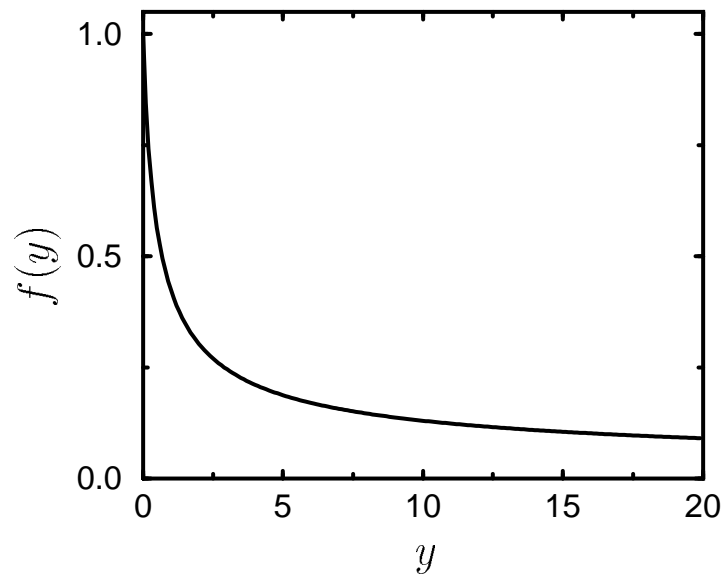
(c)

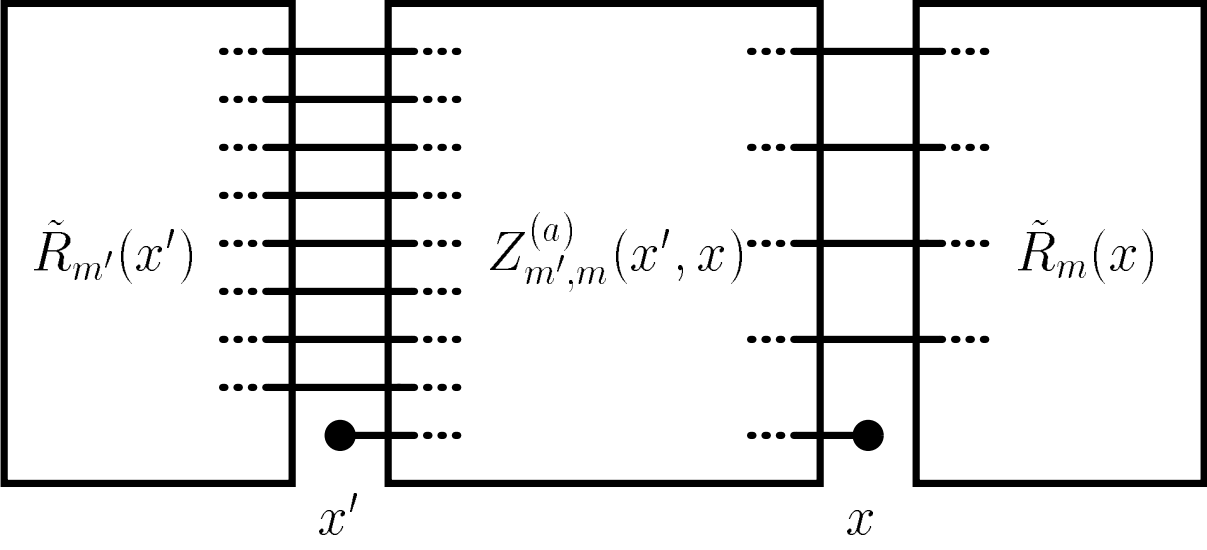


(d)

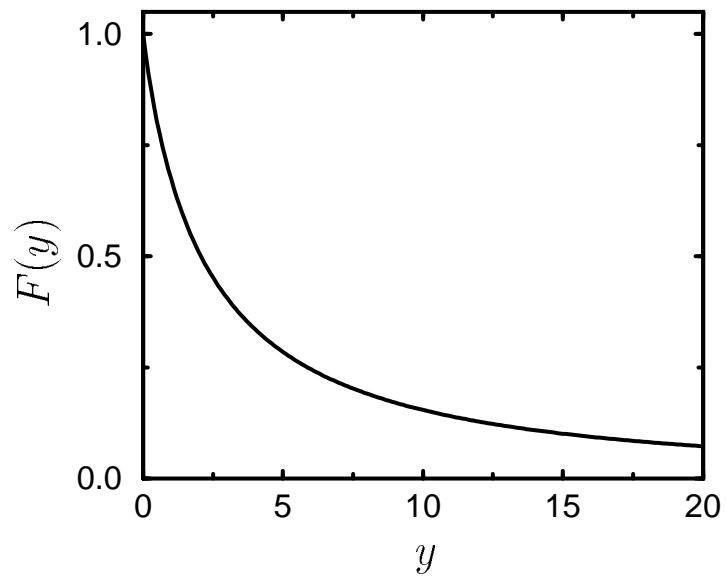


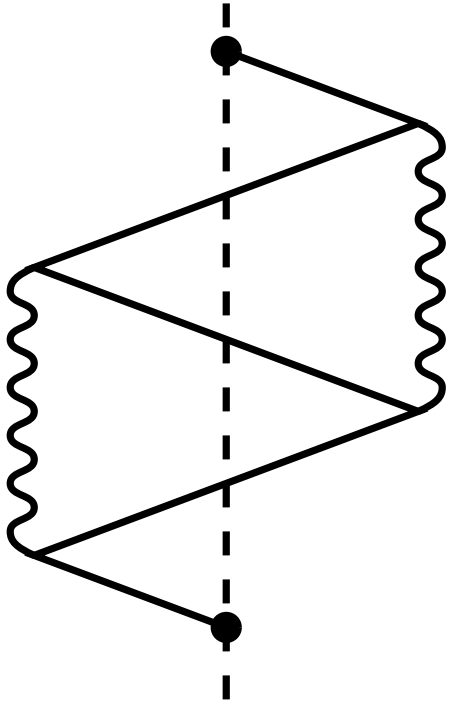




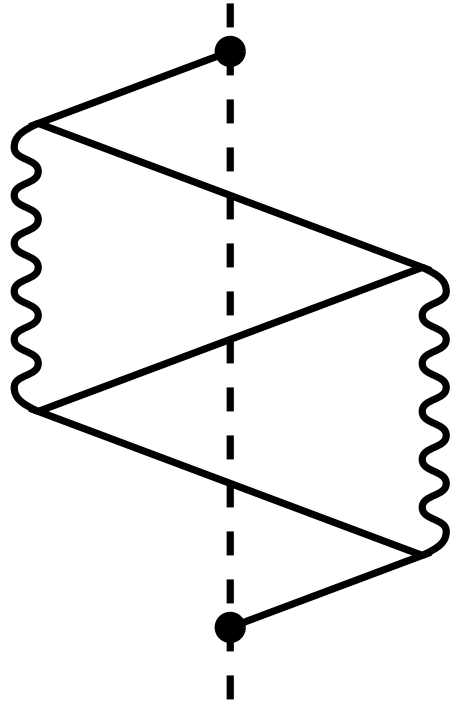


x'  (a) x  x'  (b) x  x'  (c) x  x'  (d) x 





x



x

